2023 22nd IEEE Intersociety Conference on Thermal and Thermomechanical Phenomena in Electronic Systems (ITherm) | 979-8-3503-2166-1/23/$31.00 ©2023 IEEE | DOI: 10.1109/ITHERM55368.2023.10177618

# Prediction and Flow Visualization of Critical Heat Flux of PF-5060 within a Horizontal Rectangular Channel with Single Sided Heating

Chinmay Shingote[a], Cho-Ning Huang[a], Chirag Kharangate[a]*

[a] *Department of Mechanical and Aerospace Engineering, Case Western Reserve University, Cleveland, OH 44106*

*cts49@case.edu*, cxh580@case.edu, crk91@case.edu

*Abstract* - **This study focuses on predicting and exploring the conditions leading to Critical Heat Flux (CHF) of PF-5060 within a 5mm high and 2.5mm wide horizontal rectangular flow channel. The test section allows for both top side and bottom side single-sided heating setup. The top and bottom heating results help in understanding the effect of gravity on the liquid-vapor phases and interactions. Tests were conducted on PF-5060 with inlet velocity within the range of 0.2 to 0.7 m/s. Subcooled inlet conditions were tested with an average inlet subcooling ranging from 5°C to 33°C. The fluid was heated using a custom-designed 100% oxygen free copper heater with a heated length of 114.6mm and 2.5mm width. Images of the boiling phenomena were acquired using a high-resolution camera. Images taken during this study revealed that vapor takes the form of a wavy layer which allows the liquid to stay in contact with the heated surface at intermittent intervals. The flow visualization data provides information on how changes in velocity and subcooling affect the vapor phase of the fluid. It's observed that the vapor phase size increases along the length of the heater. The size of the vapor phase decreases with higher subcooling and higher velocities. The study also provides information regarding the effects of different inlet conditions on the CHF of PF-5060. The study provides key data which is used to validate a theoretical CHF models. Two common theoretical CHF models were utilized to predict the experimental CHF data. However, each model has its own strength and weakness under some certain flow and heating conditions. This study shows good agreement between experimental results and the hydrodynamic instabilities-based CHF model by Huang et. al. [1].**

***Keywords— CHF: Critical Heat Flux, Flow Boiling, PF-5060***

## I. INTRODUCTION

### A. Introduction

Subcooled flow boiling is a complicated phenomenon utilized in many industrial heat transfer applications, including conventional and nuclear power plants. It includes many heat transfer mechanisms, and is further complicated by the two phase flow and the non-equilibrium phenomena existing between the vapor and the liquid phases [2]. Although it has been studied for many years, it is difficult to fully understand the underlying physics because of limitations on the parameters that can be simultaneously measured. A better understanding of subcooled flow boiling would allow for development of better codes and methods for predicting the flow characteristics in subcooled boiling heat transfer applications. The development of better models for subcooled flow boiling would allow for better predictions of heat transfer in practical applications. This would reduce time and costs involved in evaluating the boiling characteristics of two-phase heat transfer. New designs could also be more easily evaluated without the need for running of costly experiments. Better CFD modeling of two-phase heat transfer could also impact other technologies that utilize subcooled flow boiling such as two-phase heat exchangers and two-phase semiconductor cooling devices [3].

Gravity has a strong influence in two-phase flow and heat transfer, specifically at lower inlet velocities. Body forces resulting due to gravity are measured by buoyancy. Buoyancy affects the vapor removal from the heated wall and the liquid contact with the heated wall. The most common applications utilize the vertical upflow orientation since buoyancy aids vapor removal in the direction of liquid flow. Vapor removal causes more liquid to stay in contact with the heated wall which enhances both flow stability and CHF. Hence the vertical upflow is commonly used and most of the mechanistic models

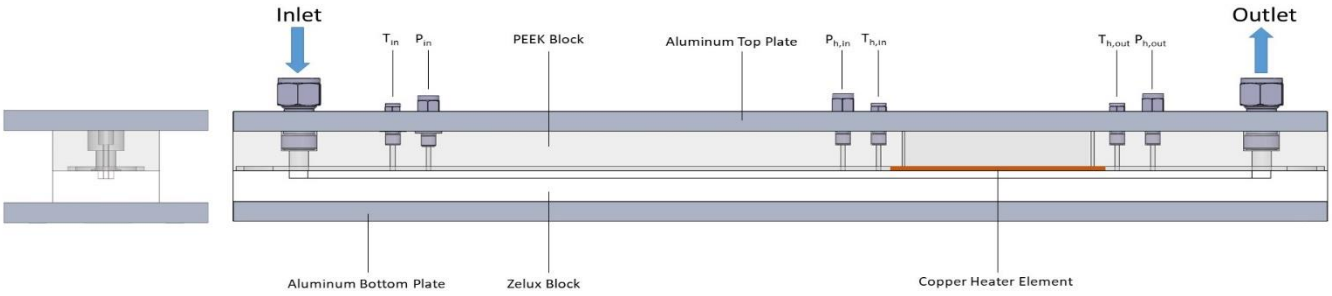


**Fig.1.** Flow Boiling Module Assembly


**Fig 2**. (a) Copper Heating Element dimensions. (b) Location of wall thermocouples

for flow boiling CHF [4-6] are intended for vertical upflow orientation.

Zhang et al. [7] performed a study based on the horizontal flow orientation with bottom wall heating for FC-72 as working fluid with subcooled inlet conditions and Kharangate et al. [8] performed the same study for saturated inlet condition. These studies showed that buoyancy aided the removal of vapor from the bottom heated surface. Whereas in top wall heating, the buoyancy causes the vapor to accumulate along the heated wall leading to lower CHF values for low velocities [9,10].

### *B. Objective of Study*

The present study explores effects of subcooled inlet conditions on CHF for a horizontal flow with top wall heating. High-speed imaging is used to better understand the effects of gravity and body forces perpendicular to the heated wall on the liquid-vapor interface. The experimental data are compared for different inlet conditions. The data is used to validate the theoretical model proposed by Huang et al. [1].

## II. Experimental Methods

### *A. Flow boiling module*

The flow boiling module is made of Zelux polycarbonate and PEEK plastic sandwich. The blocks are bound together using aluminum plates on the top and bottom side. A 2.5-mm by 5-mm rectangular flow channel is milled into the Zelux along the central line. The PEEK block is manufactured to house thermocouple and pressure Swagelok fittings. A rectangular slot is milled into the PEEK to accommodate the heater. The heater is made from oxygen-free copper. An O-ring is used to prevent leaks in between the PEEK and Zelux blocks. Another O ring is used between the heater and PEEK. The Test Section assembly is shown in Fig 2(a). A differential pressure gauge is used to measure the pressure drop across the heater element. Type-K thermocouples are used to obtain temperature data. Fluid temperatures are recorded at inlet of the test section, inlet to the heater and exit of the heater. Heater wall temperature is recorded at 7 locations along the oxygen free copper heater. Fig.2(b) shows the location of the thermocouples along the copper heater element.

The heater is 15.5mm wide, 114.6mm long and 1.04mm thick. The thickness of copper is selected based on the discussions by Zhang et al. Zhang et al. [4] discusses the minimum thickness value for copper slab to exceed 0.4mm to achieve optimal axial conduction. A 4.5mm wide groove is milled onto the copper slab to house 6 resistors. The resistors have a resistance value of 190 ±10% Ω. The resistors are soldered into the groove on the copper slab. The resistors are connected in parallel and are powered by a variable voltage power supply to generate a uniform heat flux through the copper slab. Type-K wire thermocouples are used to measure the wall temperature of the copper heater element at 7 locations. The detailed heater assembly is shown in Fig 2(b).

### *B. Flow loop*

The flow loop is designed to provide suitable inlet conditions for the working fluid PF-5060. PF-5060 is clear, colorless, and highly dielectric liquid. PF-5060 is thermally stable with a saturation temperature of 56ºC at atmospheric pressure. The schematic of the flow loop is shown in Fig.3. PF-5060 is passed through a contactor which removes dissolved

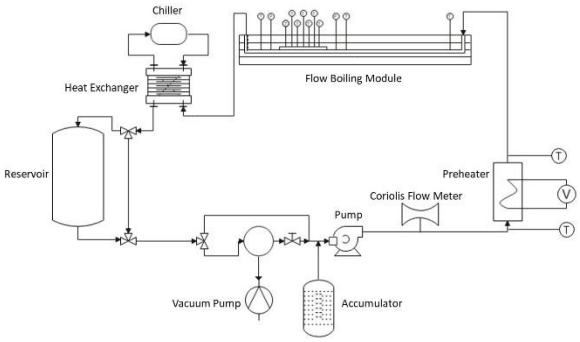


**Fig.3** Schematic of the flow loop

gases from the fluid. An accumulator is connected before the pump to main a reference pressure point in the loop. The accumulator is pressurized using compressed nitrogen which allows it to compensate for any sudden expansions or contraction in the loop. A vacuum pump is connected to the contactor to remove the gases. A magnetic drive gear pump is used to circulate PF-5060 in the loop. The pump can deliver the fluid at 0.1m/s minimum mean velocity. A Coriolis flow meter is used to obtain the flow rate information. A 1000W inline preheater is used to control the inlet fluid quality. The liquid flows through the flow boiling module turning into a two phased mixture. The mixture then flows through a high efficiency liquid to liquid heat exchanger which converts the mixture back to saturated liquid state and is reintroduced into the loop.

### C. Flow Visualization

High speed imaging is performed using a Photron Fastcam SA-Z camera. The camera has a 1 Megapixel sensor capable of obtaining ultra-slow-motion videos at 20000 fps. A wide field of view of 100mm x 8mm is utilized to visualize the heated section of the flow boiling module. Videos are captured at 20000 fps for 1 second of each test. The Flow field is illuminated using a LED light source array. The light source is placed behind the test section which illuminates the Field of View. The light from the LEDs is diffused using diffusion sheets which help is uniform illumination of the test section.

### D. Standard Operating Procedure

The flow loop is run without any heating to perform degassing of the fluid. Degassing is performed during the initial run for deaerating the fluid. The degassing is performed for 6-8 hours to ensure no dissolved gases are present in the loop. Once the degassing is achieved, the preheater is turned on to heat the fluid and achieve the required inlet subcooling. The loop controls are automated using a Labview program using a national instruments CDAQ system. The pump speed is set in Labview to desired inlet velocity. The preheater is powered using a variac to heat the fluid to desired inlet temperature. The Labview program also facilitates the measurement of Temperatures, Pressure and Flow rate of the fluid. Once the desired inlet conditions are reached, the Copper heater element is powered on using the Labview program. Power is applied in small increments, once the wall temperature of the heating element reaches steady state, the camera is triggered using the host computer to capture the video of the flow. A fail-safe is implemented into the Labview program to protect the Zelux polycarbonate from burning out. The fail-safe automatically cuts off the heater power even if one of the wall temperatures exceeds 120ºC.

### E. Measurement Accuracy

The Coriolis flow meter used to measure the flow rate has an accuracy of ±0.1%. Wall Temperature data is recorded using Type-K wire thermocouples which have an accuracy of ±0.75% or ±0.5ºC. The fluid temperature is measured using Type K Probe Thermocouples which have an accuracy of ±1ºC. The differential pressure transducer used to measure the pressure drop across the heating element has an accuracy of 0.1%, while the absolute pressure transducer used to measure the inlet pressure has an accuracy of ±0.05%.

## III. Experimental Results

### A. CHF Results

Fig.4 shows the variation of CHF for different inlet velocities with the four levels of inlet subcooling. 8.62 W/cm$^2$ is the lowest observed CHF for the lowest fluid velocity of 0.2 m/s with low subcooling of 5ºC since vapor gets stuck along the top heating element. This can be seen in the flow visualization data. The highest CHF of 32.74 W/cm$^2$ is seen at the highest velocity of 0.7 m/s with no preheating. This shows that inlet conditions of the fluid greatly affect the CHF value.

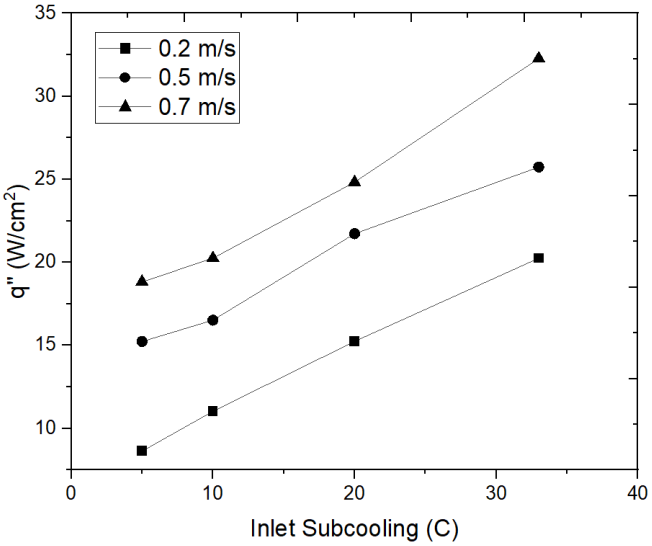


**Fig.4** CHF vs Inlet subcooling for different inlet fluid velocity.

### B. Boiling Curves

The heating element is fitted with 7 thermocouples to record the wall temperatures. The following plots show the boiling curve for the different fluid velocities. The heat flux q" is plotted against the $T_{w,\,avg}$ to show the boiling curve. The plots show a typical formation like a boiling curve. The slope increases as the liquid transitions from single phase to nucleate boiling, then reducing as it reaches CHF. The transition point differs based on the different inlet conditions. Fig 5 shows the

boiling curves for different fluid velocity with inlet subcooling of 5°C. The CHF occurs much later for higher fluid velocity which is evident by the change in slope. Fig. 6 shows the boiling curve for higher inlet subcooling of 20°C.

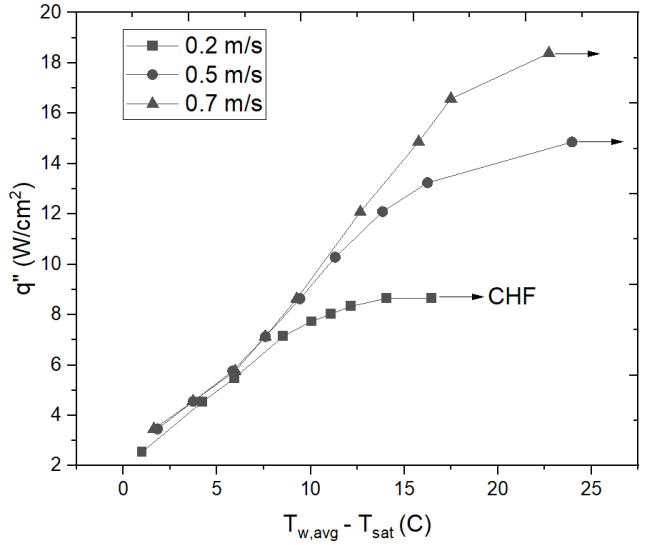


**Fig.5** Boiling Curve for inlet subcooling of 5°C.

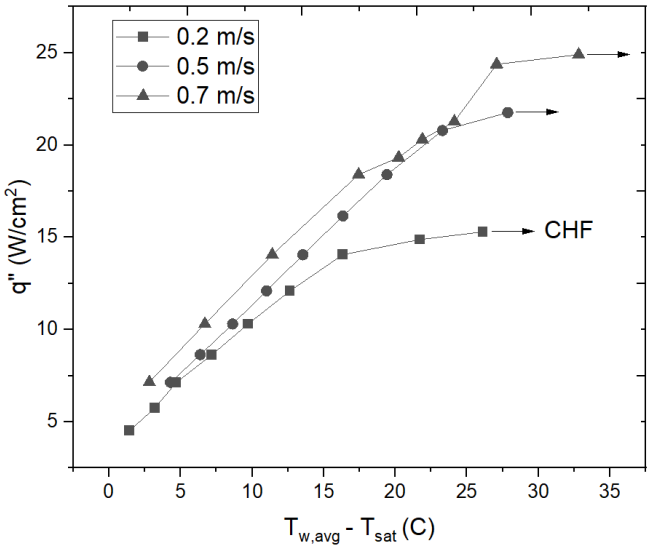


**Fig.6** Boiling Curve for inlet subcooling of 20°C.

## C. *Heat Transfer Co-efficient*

The local heat transfer coefficient at the thermocouple location can be calculated using the following equation.

$$h = \frac{q"}{(T_w - T_f)}$$

where q" is the applied wall heat flux, $T_w$ is the wall temperature measured at the heating element, while $T_f$ is the bulk fluid temperature. Fig. 7 and Fig. 8 show the heat transfer coefficient vs the wall heat flux for 5°C subcooling and 20°C subcooling respectively. The highly subcooled liquid has a larger local heat transfer coefficient. The heat transfer coefficient peaks and then drops as liquid reaches CHF.

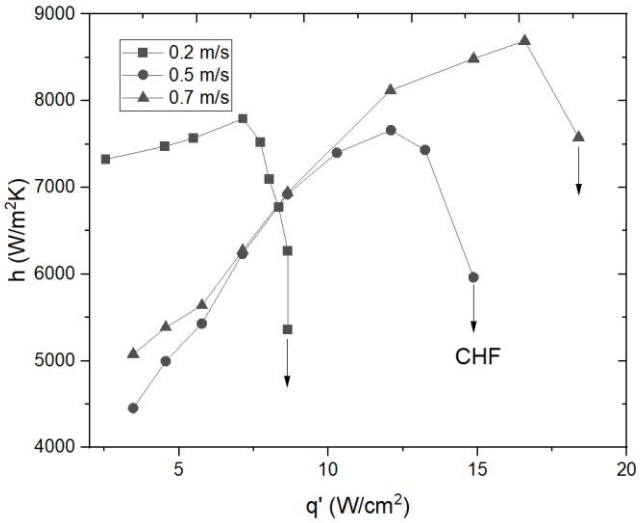


**Fig.7** Heat transfer co-efficient vs heat flux for inlet subcooling of 5°C

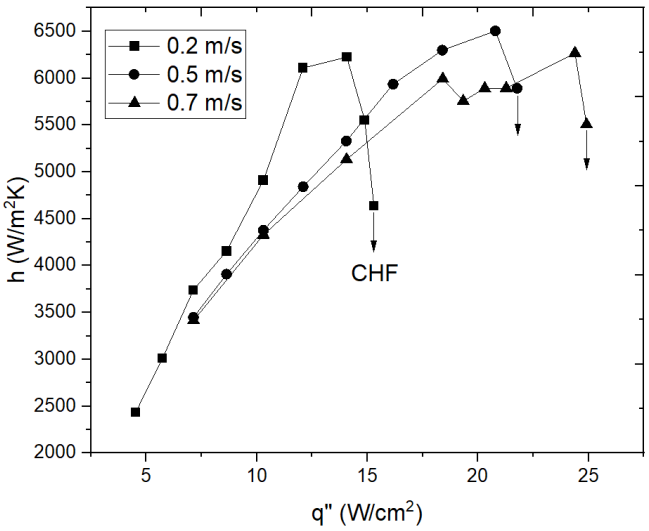


**Fig.8** Heat transfer co-efficient vs heat flux for inlet subcooling of 20°C

## D. *Verification of CHF model*

Huang et al. [1] developed a theoretical model to predict CHF in rectangular channel with single sided heating. The CHF model is based on three sub-models, which are the separated flow model, the interfacial instability critical wavelength model, and the Helmholtz wavelength model. Based on the inlet conditions, the separated flow model is implemented to determine the average velocities and thicknesses of the vapor and liquid layers along the flow channel. These velocities and phase thicknesses are utilized in conjunction with classical interfacial instability theory to calculate the critical wavelength of the liquid-vapor interface in the wetting front. Lastly, CHF is calculated based on energy balance in the wetting front region based on the Helmholtz.

The experimental data obtained in this study is used to verify the credibility of the theoretical model. The CHF values for the three inlet velocities at 5°C and 10°C subcooling is used for the comparison. The results are shown in Fig.9

Good agreements were observed between the experimental data and the predictions of the CHF model. The mean absolute error (MAE) is 20.9% and the definition of MAE is shown below.

$$MAE = \frac{1}{N}\sum\left|\frac{CHF_{pred} - CHF_{exp}}{CHF_{exp}}\right|$$

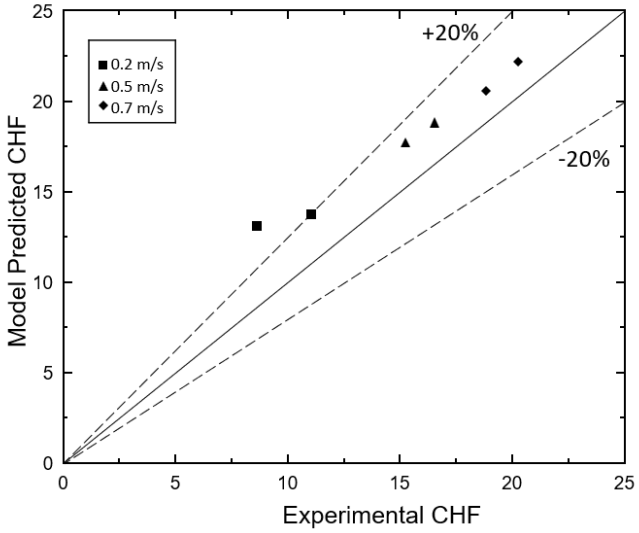


**Fig.9** Experimental CHF compared to Model Predicted CHF

## IV. Flow Visualization Results

Fig.10 shows the results for different inlet flow conditions using high speed imaging. The liquid-vapor interface can be clearly observed. The buoyancy effect can be observed as the fluid reaches CHF. The vapor starts to accumulate along the top heated wall thereby hindering the liquid contact with the heated surface, which leads to CHF.

Fig.10 shows the change in the bubble formation leading to CHF for 0.2m/s, 0.5m/s, 0.7m/s for low subcooling of 5C, medium subcooling of 10C, and high subcooling of 20C. Bubble formation occurs downstream of the inlet. Vapor rises towards the heated wall causing the liquid to lose contact with the heated wall. This is evident in the flow visualization results for all the flow rates. At lower inlet velocity, the body forces are dominant which causes more vapor to accumulate at the heated wall. This causes the lower CHF values for lower inlet velocities. The thickness of the vapor layer reduces with increase in fluid velocity. This explains the CHF value being higher with increase in fluid velocity.

0.2 m/s, 5ºC Subcooling, CHF=8.62 W/cm$^2$

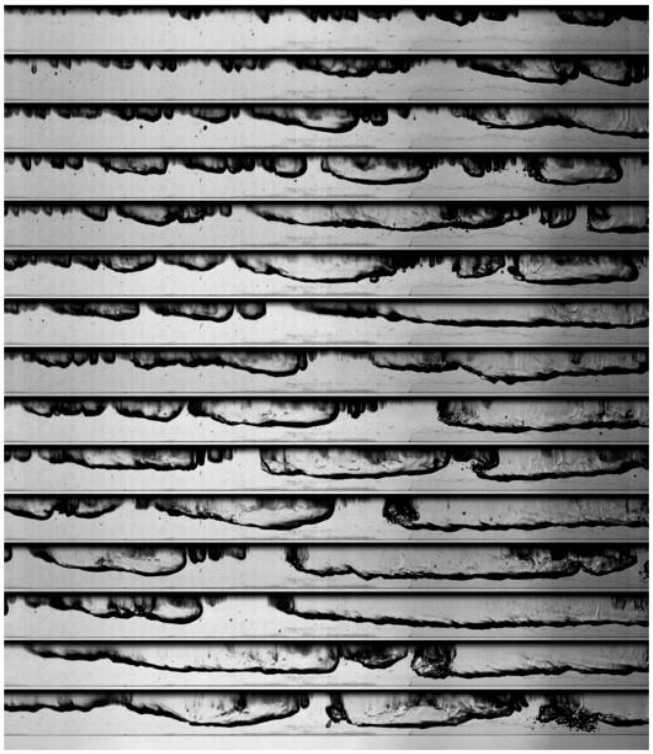

0.2m/s, 10ºC Subcooling CHF=11.03 W/cm$^2$

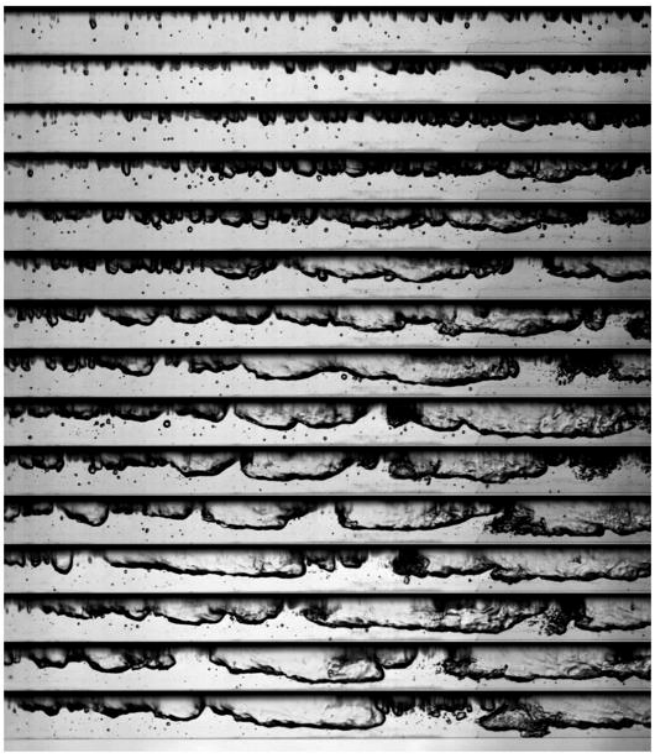

**Fig.10** High Speed Video Image Sequence leading to CHF for different inlet velocities, and subcooling.

0.2 m/s, 20°C Subcooling, CHF=15.24 W/cm$^2$

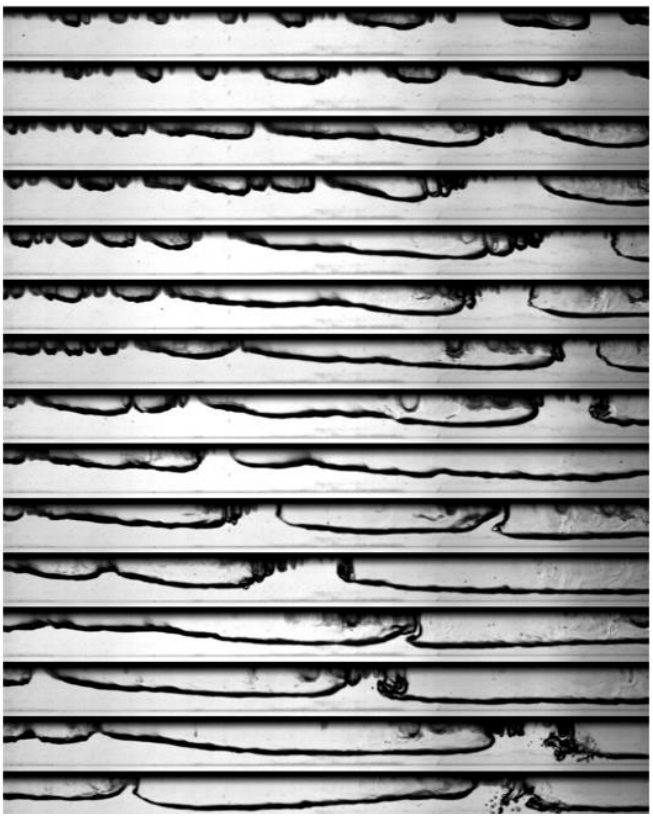

0.5m/s, 5°C Subcooling, CHF=15.23 W/cm$^2$

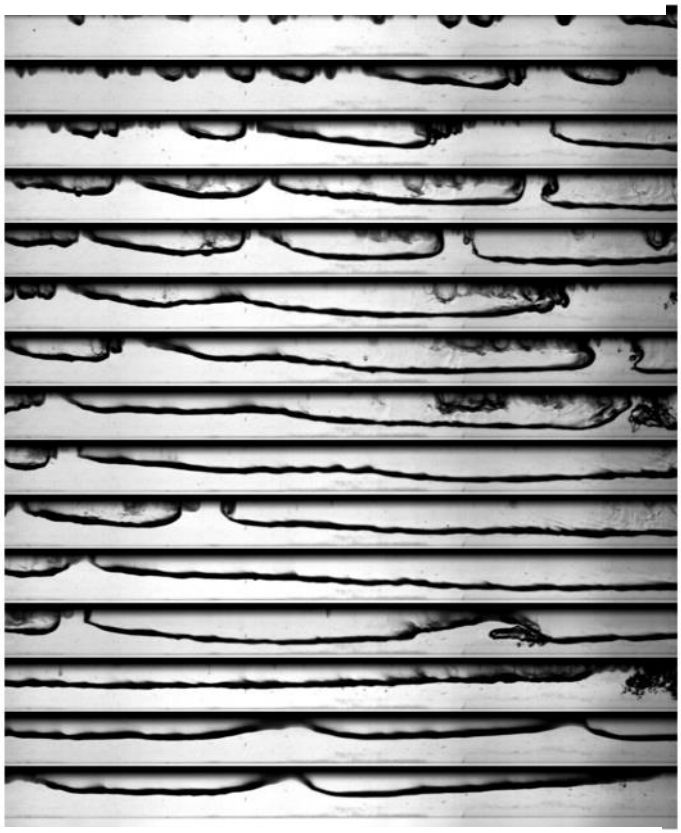

0.5 m/s, 10°C Subcooling, CHF=16.52 W/cm$^2$

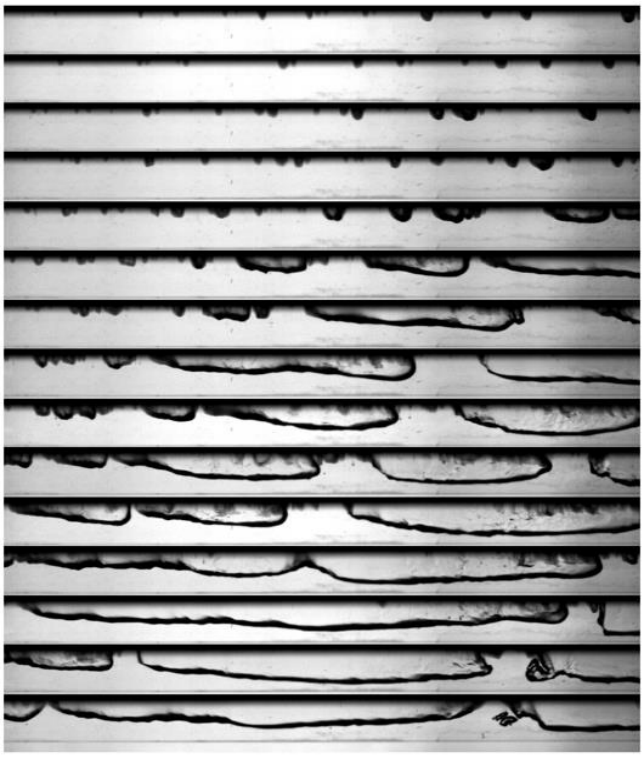

0.5m/s, 20°C Subcooling, CHF=21.72 W/cm$^2$

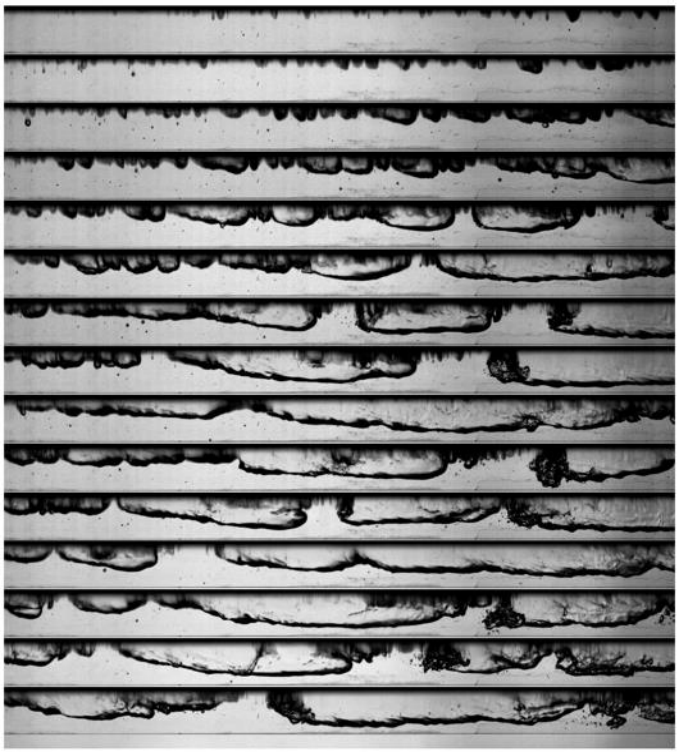

**Fig.10** High Speed Video Image Sequence leading to CHF for different inlet velocities, and subcooling. (contd.)

0.7 m/s, 5ºC Subcooling, CHF=18.82 W/cm$^2$

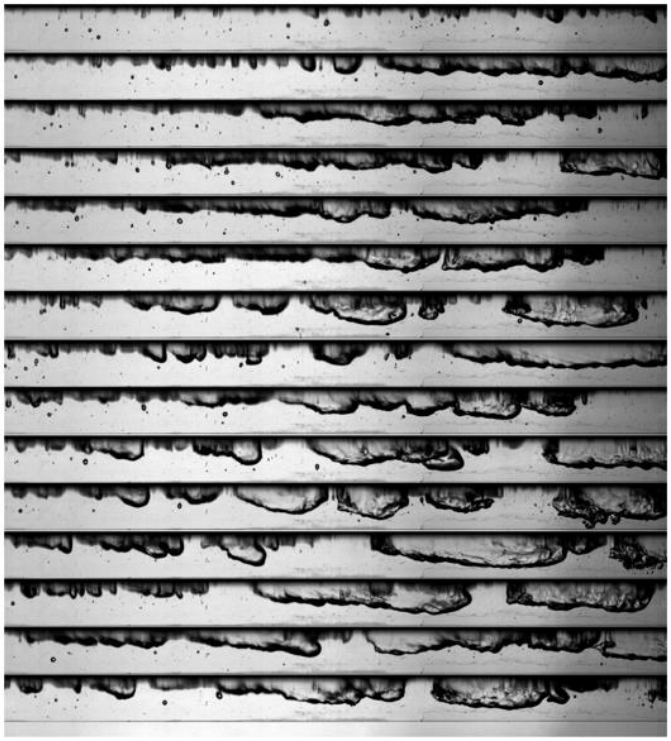

0.7m/s, 10ºC Subcooling, CHF=20.25 W/cm$^2$

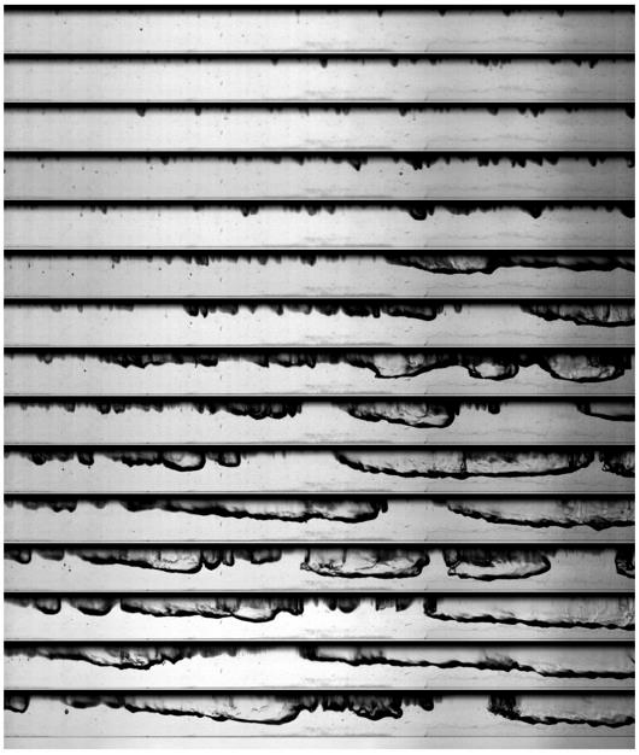

0.7m/s, 20ºC Subcooling, CHF=24.83 W/cm$^2$

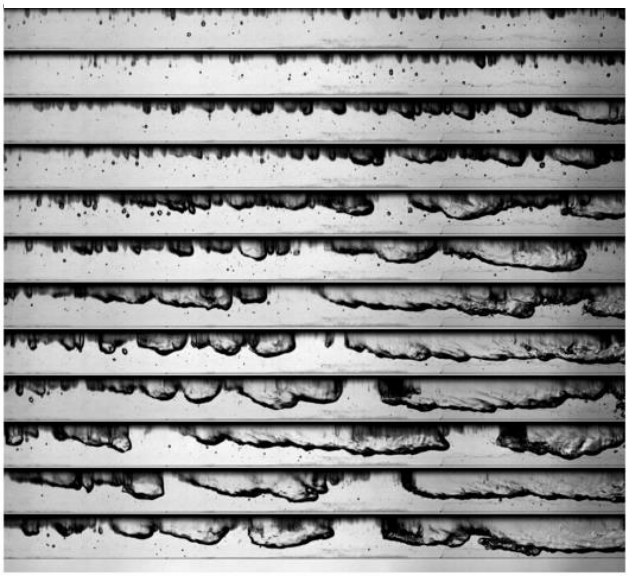

**Fig.10** High Speed Video Image Sequence leading to CHF for different inlet velocities, and subcooling (contd.)

## V. Conclusions

This study investigated CHF and conditions leading to CHF for PF-5060 working fluid. Different inlet velocities of 0.2m/s to 0.7m/s were tested. A subcooling range of 5ºC to 33ºC was used to evaluate the effect on CHF occurrence. High Speed Imaging was used to understand the interface between liquid and vapor phase. CHF is greatly affected by the inlet condition of the liquid. A highly subcooled liquid will attain CHF earlier than a non-subcooled fluid. A highly subcooled liquid will have a greater wall heat transfer coefficient than a non-subcooled fluid. Lower CHF values are observed for lower flow rates. The fluid velocity directly affects the CHF. The theoretical model proposed by Huang et al [1] was verified using the experimental data.


## Acknowledgment

The authors are thankful to Two Phase Flow and Thermal Management Lab at Case Western Reserve University for providing the support for conducting this study.


## References


[1] Cho-Ning Huang, Chirag R. Kharangate, Consolidated model for predicting flow boiling critical heat flux in single-sided and double-sided heated rectangular channels, International Journal of Heat and Mass Transfer, Volume 160, 2020, 120132, ISSN 0017-9310, https://doi.org/10.1016/j.ijheatmasstransfer.2020.120132.

[2] Two-phase micro-channel heat sinks: theory, applications and limitations, I. Mudawar, J. Electronic Packaging – Trans. ASME, 133 (2011), p. 041002

[3] Chirag R. Kharangate, Lucas E. O'Neill, Issam Mudawar, Mohammad M. Hasan, Henry K. Nahra, Ramaswamy Balasubramaniam, Nancy R. Hall, Ashley M. Macner, Jeffrey R. Mackey, Flow boiling and critical heat flux in horizontal channel with one-sided and double-sided heating, International Journal of Heat and Mass Transfer, Volume 90, 2015, Pages 323-338, ISSN 0017-9310.
https://doi.org/10.1016/j.ijheatmasstransfer.2015.06.073.
[4] S.S. Kutateladze, A.I. Leont'ev, Some applications of the asymptotic theory of the turbulent boundary layer, in: Proc. Third Int. Heat Transfer Conf., Chicago, Illinois, vol. 3, 1966, pp. 1–6.
[5] L.S. Tong, Boundary-layer analysis of the flow boiling crisis, Int. J. Heat Mass Transfer 11 (1968) 1208–1211.
[6] W. Hebel, W. Detavernier, M. Decreton, A contribution to the hydrodynamics of boiling crisis in a forced flow of water, Nucl. Eng. Des. 64 (1981) 443–445.
[7] Hui Zhang, Issam Mudawar, Mohammad M. Hasan,
CHF model for subcooled flow boiling in Earth gravity and microgravity, International Journal of Heat and Mass Transfer, Volume 50, Issues 19–20, 2007, Pages 4039-4051, ISSN 0017-9310.
[8] C.R. Kharangate, I. Mudawar, M.M. Hasan, Photographic study, and modeling of critical heat flux in horizontal flow boiling with inlet vapor void, Int. J. Heat Mass Transfer 55 (2012) 4154–4168.
[9] H. Zhang, I. Mudawar, M.M. Hasan, Experimental and theoretical study of orientation on flow boiling CHF, Int. J. Heat Mass Transfer 45 (2002) 4463–4477.
[10] C. Konishi, I. Mudawar, Investigation of the influence of orientation on critical heat flux for flow boiling with two-phase inlet, Int. J. Heat Mass Transfer 61 (2013) 176–190.